Characterization and Structural Analyses of Nonspecific Lipid Transfer Protein 1 from Mung Bean[†,‡]

Ku-Feng Lin,[§,||] Yu-Nan Liu,[§,||] Shang-Te D. Hsu,[⊥] Dharmaraj Samuel,[||] Chao-Sheng Cheng,[||] Alexandre M. J. J. Bonvin,[⊥] and Ping-Chiang Lyu*[,||]

Department of Life Sciences, National Tsing Hua University, Hsinchu, Taiwan, and NMR Department, Bijvoet Center for Biomolecular Research, Utrecht University, 3584CH Utrecht, The Netherlands

Received November 12, 2004; Revised Manuscript Received February 1, 2005

ABSTRACT: Plant nonspecific lipid transfer proteins (nsLTPs) are thermal stable proteins that are capable of transferring lipid molecules between bilayers in vitro. This family of proteins, abundant in plants, is proposed to be involved in defense, pollination, and germination; the in vivo biological function remains, however, elusive. Here we report the purification and sequencing of an nsLTP1 from mung bean sprouts. We have also determined the solution structure of this nsLTP1, which represents the first 3D structure of the dicotyledonous nsLTP1 family. The global fold of mung bean nsLTP1 is similar to those of the monocotyledonous nsLTP1 structures and consists of four α-helices stabilized by four disulfide bonds. There are, however, some notable differences in the C-terminal tails and internal hydrophobic cavities. Circular dichroism and fluorescence spectroscopy were used to compare the thermodynamics and lipid transfer properties of mung bean nsLTP1 with those of rice nsLTP1. Docking of a lipid molecule into the solution structure of mung bean nsLTP1 reveals similar binding cavities and hydrophobic interactions as in rice nsLTP1, consistent with their comparable lipid transfer properties measured experimentally.

Plant nonspecific lipid transfer proteins (nsLTPs)[1] facilitate the movement of various polar lipids across membranes in vitro (*1*). They are proposed to be involved in the formation of a protective hydrophobic layer over the plant surface (*2*) and in plant defense against pathogens (*3*, *4*) and to be implicated in pollination and germination (*5*, *6*). Elevated expression levels of nsLTPs under different environmental conditions suggested that they may be involved in responses toward stresses such as drought, heat, cold, or salt (*7*−*9*). Furthermore, high thermostability, protease resistance, and allergenic features of nsLTPs were reported (*10*). Despite the wealth of knowledge regarding their involvement in development and their ability in assisting stress managements, detailed mechanisms of their lipid transport and physiologic functions remain elusive (*1*, *11*).

Plant nsLTPs can be divided into two subfamilies according to their molecular masses, namely, nsLTP1 (molecular mass ∼9 kDa) and nsLTP2 (molecular mass ∼7 kDa) (*12*). NsLTP1 is found primarily in aerial organs (*13*), whereas nsLTP2 is expressed in roots. Both nsLTP1 and nsLTP2 are found in seeds (*11*). The three-dimensional (3D) structures of several nsLTP1s from monocotyledonous plants have been determined by nuclear magnetic resonance spectroscopy (NMR) and X-ray crystallography (*14*−*24*). No dicotyledonous nsLTP1 structure is however currently available, although a number of nsLTP1s from dicotyledonous plant species have been isolated and sequenced (*8*, *25*−*27*). Among those, the nsLTP1 from mung bean (Mb) was recently shown to exhibit antifungal and antibacterial activities (*28*). Here we report the purification, sequencing, and 3D structure determination of Mb nsLTP1 by solution NMR spectroscopy. Circular dichroism (CD) and fluorescence spectroscopy were used to characterize the thermodynamic and biological properties of the Mb nsLTP1 and compare them with that of rice nsLTP1. The observed differences in biophysical properties of nsLTP1 of Mb and rice are substantiated by comparing their sequences, 3D structures, and internal hydrophobic cavity environments in the light of their lipid transfer activity. Our results provide insight into the relationship between structure and function of dicotyledonous nsLTP1.

MATERIALS AND METHODS

Protein Purification. Rice nsLTP1 was purified from seeds (*Oryza sativa* cv. Japonica) according to previously published protocol (*29*). The same protocol was used for Mb nsLTP1 with minor modifications. Mb seeds (*Vigna radiata* var. radiate) were obtained from a local supermarket and germi-

[†] This work is supported in part by Research Grant NSC-932311B007012 from the National Science Council, Taiwan, and Program for Promoting Academic Excellence of Universities Grant 91-B-FA05-1-4 from the Ministry of Education, Taiwan. A.M.J.J.B. is a recipient of a Netherlands Organization for Scientific Research (NWO) Jonge Chemici grant.

[‡] The amino acid sequence of nsLTP1 from *Vigna radiata* var. radiate is available under SWISS-PROT accession number P83434. The assigned resonances were deposited in BMRB under accession code BMRB-6089. The atomic coordinates of the ensemble of mung bean nsLTP1 structures were deposited in the PDB under accession ID 1SIY.

* Corresponding author. Tel: +886 35722762. Fax: +886 35715934. E-mail: lslpc@life.nthu.edu.tw.

[§] These authors contributed equally in this work.

[||] National Tsing Hua University.

[⊥] Utrecht University.

[1] Abbreviations: nsLTPs, nonspecific lipid transfer proteins; Mb, mung bean; CD, circular dichroism; Gdn·HCl, guanidine hydrochloride; MRE, mean residue ellipticity; pyrPtdCho, pyrene phosphatidylcholine; Myr_2PtdGro, dimyristoylphosphatidylglycerol; RMSD, root mean squared deviation; NMR, nuclear magnetic resonance.

10.1021/bi047608v CCC: $30.25
Published on Web 03/25/2005

nated for 48 h at room temperature under high humidity. They were then homogenized with a blender and stirred for 4 h in 300 mL of acidic solution (pH 2.0). The supernatant was centrifuged at 13000 rpm for 25 min to remove insoluble particles. The pH of the supernatant was then adjusted to 7.2 with sodium hydroxide before loading onto a cation-exchange column, Sepharose (C-25) (Pharmacia, Inc.).

Low-affinity proteins were washed with a washing buffer (25 mM sodium phosphate buffer, pH 7.2) before eluting the eluent with a buffer containing 1 M sodium chloride. The solution containing the protein of interest and other basic proteins was desalted (<10 mM NaCl) and concentrated with an Amicon concentrator. Mb nsLTP1 was purified with RP-HPLC using a COSMOSIL $5C_{18}$-AR300 semipreparative column (Nacalai Tesque, Inc., Kyoto, Japan). Acetonitrile containing 0.1% (v/v) trifluoroacetic acid was used as the mobile phase. Finally, Mb nsLTP1 was eluted between 16% and 25% of acetonitrile concentration in 27 min while using a linear acetonitrile−water gradient at a flow rate of 1.5 mL/min.

Amino Acid Sequencing and Composition Analysis. The disulfide bonds of Mb nsLTP1 were reduced and modified according to the standard cysteine-modified protocols (*30*) for protein sequencing. The cysteine-modifying reagents, iodoacetic acid and 4-vinylpyridine, were purchased from Sigma-Aldrich. Trypsin and Glu-C proteases were bought from Merck and Roche Applied Science, respectively. Iodoacetic acid modified Mb nsLTP1 (500 μg) was digested with 12.5 μg of trypsin in 1 mL of 100 mM Tris-HCl (pH 8.8). Similarly, 300 μg of 4-vinylpyridine alkylated protein was digested by 2.5 μg of Glu-C in 200 μL of 100 mM sodium phosphate buffer (pH 7.8). After 2 h incubation, the tryptic peptides were separated by RP-HPLC using a COSMOSIL $5C_{18}$-AR-II analytical column with a linear gradient of 0−18% acetonitrile in 180 min and 18−38% in 30 min, at a flow rate of 1 mL/min. A similar procedure was followed after 8 h of Glu-C digestion, except for the linear acetonitrile gradient of 0−32% in 32 min, at a flow rate of 1 mL/min. The purified peptides were sequenced with automated Edman degradation methods (*31*) using MilleGen 6600 pulsed liquid protein sequencing systems. The molecular masses and amino acid compositions of the intact protein and various digested peptides were determined as described previously (*29*). The theoretical molecular mass was computed with PeptideMass (http://tw.expasy.org/tools/peptide-mass.html).

Circular Dichroism (CD) Experiments. The protein quantitation was carried out using bicinchoninic acid assay with bovine serum albumin as standard (Pierce Chemical Co., Chester, U.K.) (*32*). All CD spectra were recorded with an Aviv 202 spectropolarimeter using a 1 mm path length cuvette with protein concentrations of 16 μM. CD data were processed using KaleidaGraph (Synergy software). The solvent−substrate spectra except for chemical-induced unfolding were expressed in terms of mean residue ellipticity $[\theta]$ (MRE) in deg·cm^2·dmol^{-1} from the ellipticity values in millidegrees (θ). Chemical- and temperature-induced unfoldings of the protein were monitored by the changes in the ellipticity signal at 222 nm.

Individual CD spectra were averaged over three scans with a 0.5 nm step size with wavelengths ranging from 260 to 190 nm. The fraction of helical content (f) was calculated using the equation (*33*)

$$f = -\frac{[\theta]_{obs} n}{40000(n-4)} \times 100 \quad (1)$$

where n is the number of amino acids and θ the observed ellipticity value at 222 nm. The thermal denaturation curve was obtained with Mb nsLTP1 in 10 mM phosphate buffer at pH 7.0. The spectra were recorded from 20 to 96 °C with a 2 °C increment. Chemical-induced unfolding of Mb and rice nsLTP1s was monitored with proteins in 10 mM phosphate buffer with increasing concentration of guanidine hydrochloride (Gdn·HCl) from 0 to 7 M. Protein solutions were equilibrated with various Gdn·HCl concentrations for 16 h at 25 °C prior to measurements. The reversibility of the protein folding was tested by recording CD spectra after dilution of Gdn·HCl content. The unfolding curves were fitted to a nonlinear least-squares analysis using the equation (*34*)

$$Y = \frac{Y_F + m_F[D] + (Y_U + m_U[D])e^{-(\Delta G°(H_2O) + m_G[D])/RT}}{1 + e^{-(\Delta G°(H_2O) + m_G[D])/RT}} \quad (2)$$

where Y is the value of the spectroscopic property of protein at a given Gdn·HCl concentration [D], Y_F and Y_U denote the intercepts, m_F and m_U are the slopes of the baselines of the native and unfolded states, respectively, m_G is a measure of the dependence of $\Delta G°$ on [D], and $\Delta G°(H_2O)$ is the free energy change in the absence of denaturant.

NMR Experiments and Assignments. All NMR experiments were carried out using a purified Mb nsLTP1 sample dissolved in 20 mM phosphate buffer (90% H_2O and 10% D_2O, pH 3.0) reaching a final sample concentration of 3 mM. Sodium 3-(trimethylsilyl)[2,2,3,3-$^2H_4$]propionate (TSP-d_4) was added as the internal standard. Homonuclear two-dimensional total correlation spectroscopy (TOCSY) and nuclear Overhauser enhancement spectroscopy (NOESY) spectra were recorded at 25 °C on a Bruker AVANCE 600 MHz NMR spectrometer. The TOCSY spectra were recorded at 80 ms mixing time whereas the NOESY spectra were recorded at 100, 150, and 200 ms mixing time. All spectra were recorded with 512 t_1 increments and 2048 t_2 complex data points processed using XWIN-nmr (Bruker) and analyzed using SPARKY (*35*). The assigned resonances were deposited in BMRB under accession code BMRB-6089. Distance restraints were derived from the NOESY spectrum recorded with a 100 ms mixing time. A TOCSY spectrum was recorded after dissolving the lyophilized Mb nsLTP1 in 99% D_2O at 25 °C for 36 h to identify the protected amide protons.

Structural Calculation and Analysis. Peak lists and chemical shift lists were obtained from manual assignment using the SPARKY program. The peak intensities were derived using the default peak fitting protocol assuming Lorenzian line shapes. The structure calculations of Mb nsLTP1 were carried out using CNS 1.1 (*36*) and ARIA 1.2 (*37*) with torsion angle dynamics (TAD) and standard simulated annealing protocols. It was followed by explicit water refinement using the OPLS water model (*38*). Twelve structures with lowest total energies out of 200 structures

(A)

	Sequence /residue number	Mw (Experimental)	Mw (Theoretical)
Peptide T1	TTADRR / 40-45	719.4	719.4
Peptide T2	AAAGAVR / 53-59	615.4	615.3
Peptide T3	ISTSTNCNSIN / 81-91	1211.6	1211.5
Peptide T4	NILNSSR / 33-39	803.5	803.4
Peptide T5	AVCSCLK / 46-52	839.4	839.4
Peptide T6	GINPNNAEALPGK / 60-72	1294.9	1294.7
Peptide T7	GGVVPPSCCTGVK / 20-32	1319.7	1319.6
Peptide T8	CGVNIPYK / 73-80	951.6	951.5
Peptide T9	MTCGQVQGNLAQCIGFLQK/ 1-19	2155.0	2155.0
Peptide G1	ALPGKCGVNIPYKIS…/ 68-91	2705.1	2705.1
Peptide G2	MTCGQVQGNLAQCIGFLQKGGVVPPSC CTGVKNILNS…/ 1-67	7452.5	7452.8

(B)

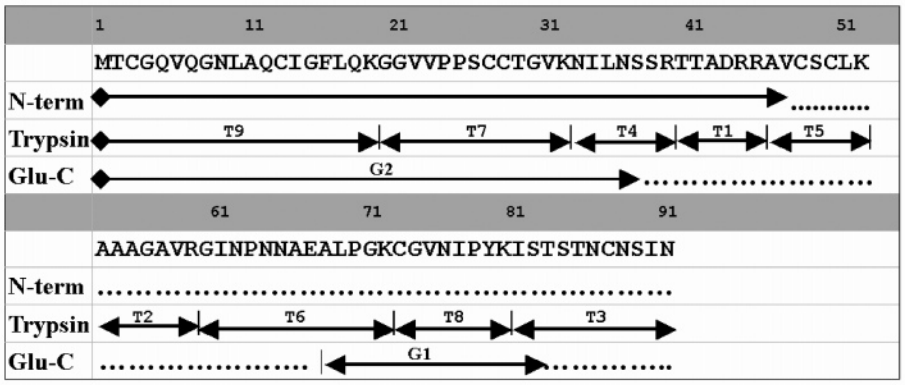

FIGURE 1: Sequence analysis of Mb nsLTP1. (A) Amino acid sequences and corresponding molecular weights of trypsin and Glu-C digested fragments of Mb nsLTP1. (B) Peptide mapping of the Mb nsLTP1. T and G represent the fragments obtained by trypsin and Glu-C digestion, respectively. The residue number denotes positions of fragments in the protein sequence. Double-headed arrows denote N-terminal sequencing of the digestic fragments. Incomplete sequencing of a few peptide fragments is indicated with dots.

were selected for analyses. Their quality was assessed using PROCHECK-nmr (*39*). The atomic coordinates of the ensemble of structures were deposited into the PDB under the accession ID 1SIY. Superimposition of Mb onto maize (PDB ID: 1MZL), rice (PDB ID: 1RZL), wheat (PDB ID: 1GH1), and barley nsLTP1s (PDB ID: 1LIP) was obtained by least-squares positional fitting on backbone atoms of the whole protein (except the Ala^1 and Gln^{21} in maize nsLTP1) using Swiss-Pdb Viewer v3.6 (*40*). The location and volume of the hydrophobic cavity were calculated using Voidoo, with a 1.4 Å probe radius and a 1.05 scaling factor for the van der Waals radii (*41*). If present, the ligand was removed before calculation. Atomic coordinates, rotated into six directions, were used for calculation of cavities. The solvent-accessible surfaces of rice and Mb nsLTP1s were calculated using MSMS (*42*), with a 1.5 Å probe radius and a 1.0 vertex/$Å^2$ triangulation density. Molecular modeling was conducted using the DOCKING module of the Insight II software package (Molecular Simulations, Inc.) with the AMBER force field. Coordinates for the ligand (myristate) were obtained from the structure of the maize nsLTP1−myristate complex (PDB ID: 1FK2). The myristate molecule was docked into the hydrophobic cavity of Mb nsLTP1, the putative binding site. The structure of the ligand was further optimized by allowing structural flexibility after translation and rotation within the cavity. The conformation with the lowest intermolecular energy was chosen for further refinement using the Discover 3 module in Insight II and subjected to 1000 steepest descent energy minimization steps. Protein−ligand interactions were analyzed using Ligplot v.4.0 (*43*).

Lipid Transfer Assay. Lipid transfer activities were assayed by fluorescence spectroscopy as described previously (*44*). Two microliters (0.118 mM) of pyrPtdCho and 10 μL (1 mg/mL) of Myr_2PtdGro were solubilized in ethanol and mixed in a cuvette containing 8 μM protein in 2 mL of 20 mM Tris-HCl/5 mM EDTA buffer (pH 7.4). Fluorescence intensities were monitored at 396 nm with excitation at 346 nm using a Perkin-Elmer LS 55 luminescence spectrometer at 25 °C.

RESULTS AND DISCUSSION

Primary and Secondary Structure. The primary sequence of Mb nsLTP1 was established using N-terminal sequencing of the cysteine-alkylated Mb nsLTP1 and fragments obtained from proteolytic digestions (Figure 1A). Analysis of the first 47 residues of the cysteine-modified protein confirmed the presence of four conserved cysteines at positions 3, 13, 27, and 28. Trypsin digestion gave nine fragments which were designated T1−T9 according to their elution order. On the basis of the molecular weights, protein sequences, and amino acid composition analysis of these tryptic products, we

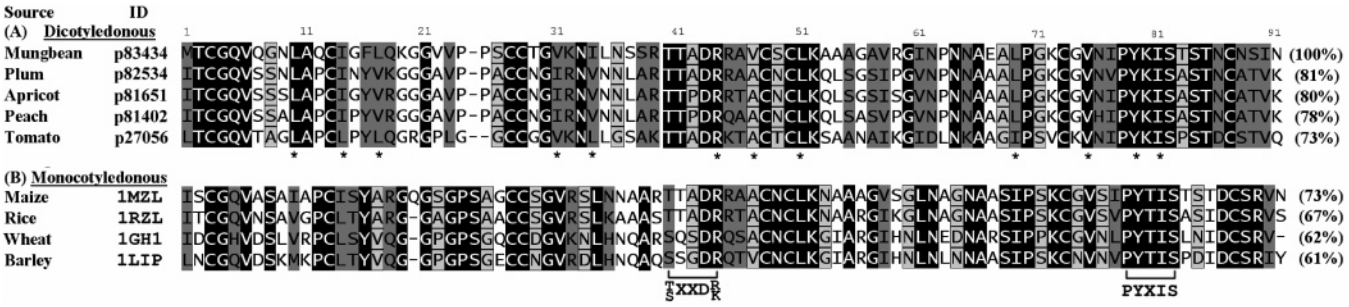

FIGURE 2: Sequence alignment of various nsLTP1s. (A) Dicotyledonous nsLTP1s. (B) Monocotyledonous nsLTP1s. Various nsLTP1 sequences of dicotyledonous (p83434, p82534, p81651, p81402, and p27056) and monocotyledonous (1MZL, 1RZL, 1GH1, and 1LIP) plants were obtained from SWISS-PROT and the PDB database, respectively. Identical residues are highlighted by dark background; conserved and semiconserved residues are shaded and boxed, respectively. Sequence similarities (within parentheses) were derived by BLAST (http://www.ncbi.nlm.nih.gov/BLAST/). Residues involved in ligand binding (*15*, *18*, *20*, *24*) are indicated with an asterisk. The two consensus pentapeptides (T/S-X-X-D-R/K and P-Y-X-I-S) that have been proposed to be important for catalysis or binding (*11*) are indicated at the bottom.

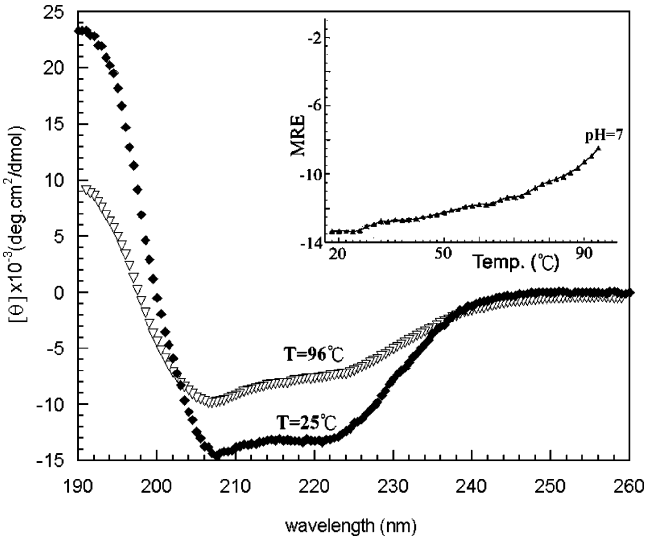

FIGURE 3: Far-UV CD spectra of Mb nsLTP1 at 25 and 96 °C. The inset shows the thermal denaturation curves monitored by CD at 222 nm in the same buffer (pH 7.0).

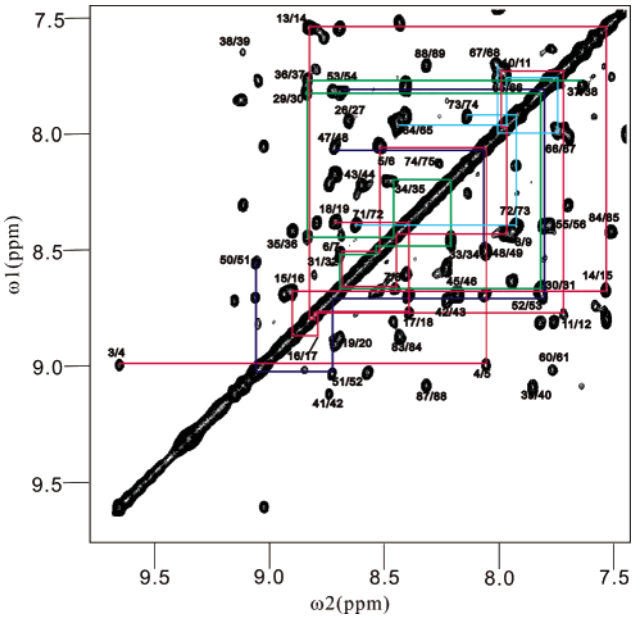

FIGURE 4: Expended NOESY spectrum of Mb nsLTP1 with sequential assignments of H^N-H^N cross-peaks. The red lines correspond to the assignment in helix I, green lines to helix II, blue lines to helix III, and cyan lines to the helix IV. The NOESY spectrum of Mb nsLTP1 shown here was measured at 298 K with a mixing time of 100 ms. The protein sample was dissolved in 20 mM phosphate buffer (pH 3.0) containing 90% H_2O and 10% D_2O.

concluded that fragments T9, T7, T4, T1, and partially T5 comprise the first 47 residues. The arrangement of the remaining fragments (T2, T3, T6, and T8) was delineated by means of Glu-C digestion (Figure 1A) which leads to specific cleavage at the carbonyl end of glutamate residues. The modified Mb nsLTP1 was cleaved into two peptides, G1 and G2, with corresponding molecular masses of 2705 and 7453 Da, respectively. Sequencing the first 15 residues of peptide G1 allowed us to arrange T6-T8-T3 in order, and the complete primary structure of Mb nsLTP1 was thus obtained (Figure 1A).

Mb nsLTP1 contains 91 amino acids including eight cysteine residues (positions 3, 13, 27, 28, 48, 50, 73, and 87) (Figure 1B) and includes two conserved pentapeptides among nsLTP1 family members, TTADR (residues 41−45) and PYKIS (residues 79−83). It has been proposed that these two consensus pentapeptides (T/S-X-X-D-R/K and P-Y-X-I-S) are important for catalysis or binding (*11*). The primary sequence of Mb nsLTP1 shares high sequence similarity (60−80%) with other nsLTP1s (Figure 2).

Mb nsLTP1 shows a typical α-helical CD spectrum at 25 °C (double minima at 222 and 208 nm and a maximum at 195 nm) (Figure 3) with a helical content of 33 ± 2%, according to eq 1 with MRE value $[\theta]_{222}$ of −12500 ± 500 deg·cm^2·dmol^{-1}. Mb nsLTP1 was found to be very stable to heat denaturation at neutral pH as shown in the inset of Figure 3.

Assignment of NMR Spectra and Structure Calculation of Mb nsLTP1. Proton resonance assignment of the purified Mb nsLTP1 was completed using standard protocol (*45*). Representative sequential assignments and NOE connectivities in the H^N-H^N region are shown in Figure 4. In total, 1595 distance restraints were derived from cross-peaks in the 100 ms NOESY spectrum (Table 1). The abundant *i* to *i* + 3 and *i* to *i* + 4 NOE connectivities and slow amide proton exchange rates (Supporting Information) are in agreement with the high helical content observed in the CD spectrum (Figure 3). Four conserved disulfide bonds (Cys^3-Cys^{50}, $Cys^{13}-Cys^{27}$, $Cys^{28}-Cys^{73}$, and $Cys^{48}-Cys^{87}$) among plant LTP1s were confirmed by the corresponding long-range NOEs and were introduced subsequently as distance restraints in structure calculation. Twelve structures of Mb nsLTP1

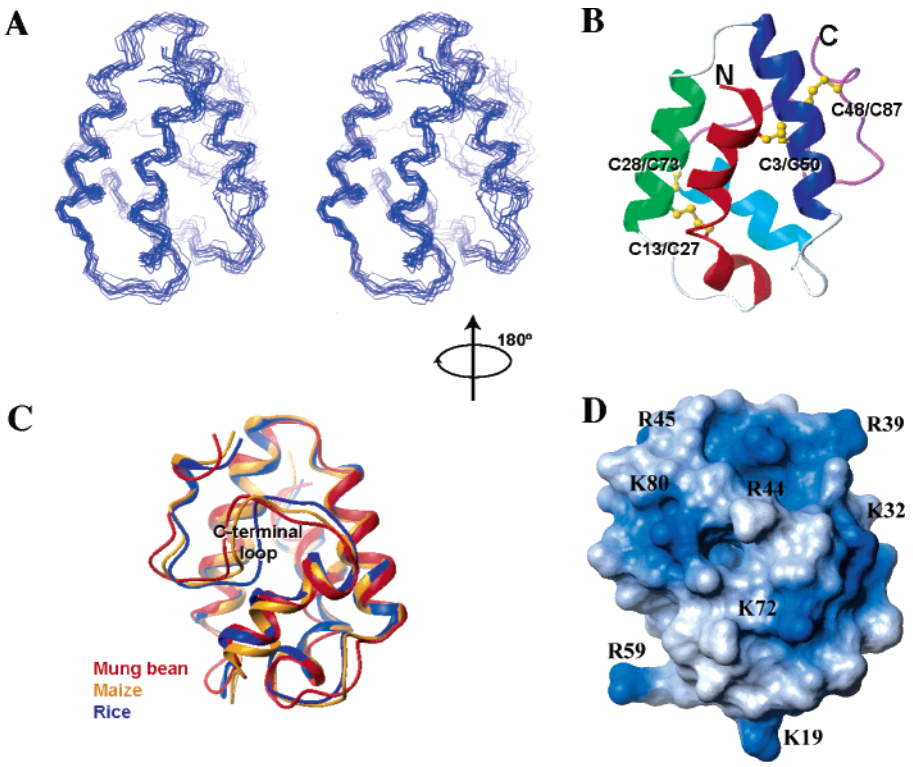

FIGURE 5: Solution structure of Mb nsLTP1. (A) Ensemble of 12 lowest energy structures. The structures were fitted on the backbone atoms of the secondary structure elements. (B) Ribbon representation of the representative structure (closest to average) of Mb nsLTP1. Helix I (Cys^3−Lys^{19}), helix II (Ser^{26}−Asn^{36}), helix III (Thr^{41}−Gly^{56}), helix IV (Pro^{63}−Cys^{73}), and the C-terminal tail are colored in red, green, blue, turquoise, and purple, respectively. The disulfide bonds are shown in ball-and-stick representation with the corresponding residue numbers. (C) Superposition of nsLTP1s of mung bean (red), maize (yellow), and rice (blue). The structures were superimposed on backbone atoms. (D) Distribution of positive charges on mung bean nsLTP1. Structures in the lower panel are rotated by 180° around their *x*-axis compared to those in the upper panel.

Table 1: Structural Statistics of Mb nsLTP1 in Aqueous Solution at pH 3.0 and 298 K[a]

experimental constraints	
total	1596
intraresidue	768
sequential ($\|i-j\|=1$)	381
medium range ($\|i-j\|\leq 3$)	288
long range ($\|i-j\|>3$)	158
RMSD from experimental data	
distance (Å)	0.019 ± 0.002
RMSD (Å) with respect to average structure	
well-defined region[b]	
backbone	0.75 ± 0.12
heavy atoms	1.12 ± 0.12
all residues	
backbone	1.30 ± 0.33
heavy atoms	1.67 ± 0.38
E_{total} after water refinement (kcal·mol^{-1})[c]	−3236 ± 72
RMSD from idealized covalent geometry	
bonds (Å)	0.0036 ± 0.0002
angles (deg)	0.484 ± 0.026
impropers (deg)	1.514 ± 0.139
Ramachandran analysis	
residues in most favored regions (%)	82.7
residues in additionally allowed regions (%)	14.3
residues in generously allowed regions (%)	1.7
residues in disallowed regions (%)	1.4

[a] The statistics are obtained from an ensemble of 12 lowest energies structures out 200 calculated ones after water refinement. [b] The well-defined region (residues 3−38, 43−53, and 59−77) was defined according to the default protocol within the ARIA package. [c] The nonbonded energies were calculated using OPLS parameters (*63*) with an 8.5 Å cutoff.

with lowest energies were chosen for structural analysis (Figure 5A). The root mean squared deviation (RMSD) values with respect to the average structure for all backbone (N, Cα, C′) and all heavy atoms are 1.3 ± 0.3 and 1.7 ± 0.4 Å, respectively (Table 1). Mb nsLTP1 contains four α-helices with an unstructured C-terminal tail (Figure 5B). The first three helices are nearly parallel, whereas the fourth is shorter and perpendicular to the first one. This structure is stabilized by four disulfide bonds which respectively connect helix I to helix III (Cys^3−Cys^{50}), helix I to helix II (Cys^{13}−Cys^{27}), helix II to helix IV (Cys^{28}−Cys^{73}), and helix III to the C-terminal tail (Cys^{48}−Cys^{87}).

The structure ensemble shows good convergence with no distance violations above 0.5 Å (Table 1). PROCHECK analysis reveals that 97% of the residues fall into the most favorable and additionally allowed regions of the Ramachandran plot (Table 1). Few residues fall into the disallowed region in the Ramachandran plot [residue Thr^2 (3), Cys^3 (1), Arg^{39} (2), Ala^{57} (1), Tyr^{79} (1), Lys^{80} (3), and Ile^{81} (1)]; their occurrence (indicated in parentheses) in the 12 selected structures is low. All these residues, except Cys^3, reside in loop regions.

Comparison with Homologous nsLTP1s. Mb nsLTP1 is highly homologous to other members of the nsLTP1 family (Figure 2). While Pro^{12}, Pro^{24}, Pro^{70}, and Pro^{78} are highly conserved in all nsLTP1s, Pro^{12} (within an intervening 3_{10} helix in helix I of rice nsLTP1) is replaced by a glutamine residue in Mb. In addition, Tyr^{16}, conserved among all other nsLTP1s, is replaced by a phenylalanine residue in Mb nsLTP1. Among the 11 charged residues of Mb nsLTP1, 7 residues (Lys^{32}, Arg^{39}, Asp^{43}, Arg^{44}, Arg^{45}, Lys^{52}, and Lys^{72}) are highly conserved, forming a positively charged patch on

Table 2: Backbone RMSD Values (Å) among Mb and Monocotyledonous nsLTP1s

	all (residues 1−91)	helices (residues 1−74)	C-terminal tail (residues 75−91)
maize[a]	2.0 ± 0.3	1.8 ± 0.2	2.6 ± 0.8
rice	2.2 ± 0.3	1.8 ± 0.2	3.3 ± 0.7
wheat	2.4 ± 0.2	2.1 ± 0.1	4.0 ± 0.8
barley	2.5 ± 0.2	2.2 ± 0.2	4.0 ± 0.8

[a] For structural comparability, Ala^{1} and Gln^{21} were deleted. The corresponding structural regions of maize nsLTP1 are all (residues 1−93), helices (residues 1−76), and C-terminal tail (residues 77−93).

the surface (Figure 5D). Notably, a number of highly conserved residues in monocotyledonous nsLTP1s are replaced in dicotyledonous nsLTP1 (Figure 2). For example, Gly^{23}, Gly^{57}, Ser^{68}, Thr^{80}, and Arg^{89} are replaced by Val, Ser/Ala, Ala, Lys, and Thr/Ser, respectively.

Several experimentally determined structures of nsLTP1/lipid complexes have revealed that the hydrophobic ligands are inserted into the internal cavity of nsLTP1s (*15*, *18*, *20*, *24*). The volume of the hydrophobic cavity varies depending on the nature of the lipid molecules (*24*). Although Ace-AMP and HPS display a comparable global fold with respect to that of nsLTPs, the lack of a hydrophobic cavity makes them unable to carry lipids in vitro (*46*, *47*). Structural analysis of nsLTP1−lipid complexes shows that residues in close contact with the lipid molecule are highly conserved. These highly conserved residues, indicated with an asterisk in Figure 2, are also observed in Mb nsLTP1. They form a tunnel-like hydrophobic cavity through the protein, suggesting that Mb nsLTP1s are capable of transferring lipid molecules.

Among several monocotyledonous nsLTP1s, the sequences of maize and rice nsLTP1s are the closest to Mb nsLTP1 (~70% similarity; see Figure 2). The 3D structure of Mb nsLTP1 therefore highly resembles that of maize and rice nsLTP1s (Figure 5C). Pairwise positional backbone RMSD values among Mb and selected monocotyledonous nsLTP1s are listed in Table 2. These nsLTP1s exhibit similar arrangement of their helices with some deviations in the C-terminal tails. Comparing with rice nsLTP1, the conformational changes of the C-terminal loop of Mb nsLTP1 (Figure 5C) result in a larger hydrophobic cavity volume. The hydrophobic cavity volume of the NMR ensemble of Mb nsLTP1 is 510 ± 45 $Å^3$, while it is only 330 ± 44 $Å^3$ for rice nsLTP1, which is 180 $Å^3$ less than that of Mb nsLTP1 (Table 3).

It has been reported that the C-terminal tail region of nsLTP1s undergoes significant conformational changes upon

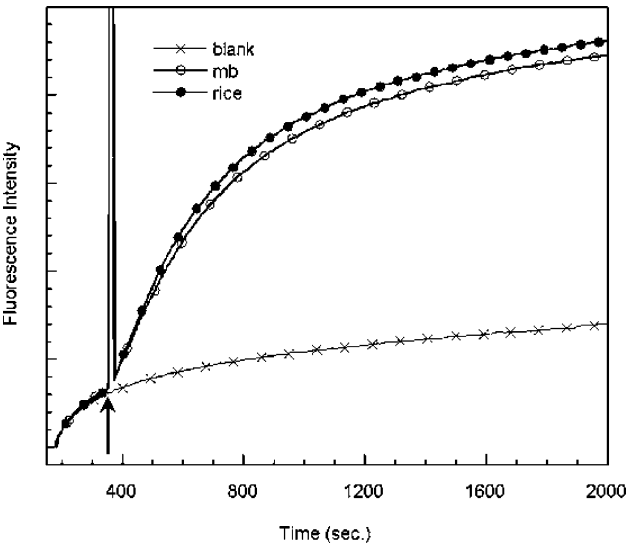

FIGURE 6: Lipid transfer assays between donor and acceptor liposomes. Protein solutions were injected at the time point of 360 s into a solution containing two vesicle populations (shown with an arrow). The fluorescence intensity increased as the protein catalyzed the shuffling of lipid molecules between the vesicles. The fluorescence intensity reaches a plateau when the fluorescent lipid molecules are equally distributed between the vesicles.

ligand binding (*24*, *48*). Tyr^{79}, Ile^{81}, and Arg^{44} are thought to be crucial for lipid binding or transfer activities of nsLTP1s (*24*, *48*). Arg^{44} resides in the conserved motif (T/S-X-X-D-R/K) of helix III in all nsLTP1s, while Tyr^{79} and Ile^{81} are located in the other conserved region (P-Y-X-I-S) in the C-terminal tail. Our solution structure of Mb nsLTP1 reveals that Arg^{44} and Tyr^{79} are located near the entrance of the hydrophobic cavity and interact with the polar headgroup of lipid molecules. Ile^{81} locates near the bottom of the lipid binding cavity, in which it may interact with the aliphatic chain of the lipid. The same interaction mode has been observed in rice nsLTP1. By contrast, Tyr^{79} and Ile^{81} of Mb nsLTP1 show different orientations as compared to that of rice nsLTP1. The Cα atoms of Tyr^{79} and Ile^{81} of Mb nsLTP1 deviate from that of rice nsLTP1 by 3.4 and 3.6 Å, respectively (calculated after superposition of all backbone atoms). These two side chains point away from hydrophobic cavity, creating a larger cavity volume.

Lipid Transfer Activity and Docking of a Lipid Molecule into Mb nsLTP1. In vitro studies have shown that nsLTP1s can transfer and/or exchange various phospholipids and glycolipid molecules across membranes (*1*). The binding/transfer activity was thought to be related to the organization of the hydrophobic cavity (*49*). The lipid transfer activities

Table 3: Physical Properties of Rice nsLTP1 and Mb nsLTP1

parameter	rice nsLTP1			Mb nsLTP1		
molecular mass (Da)	8901			9290		
no. of amino acids	91			91		
p*I*	9.41			9.25		
thermodynamic properties	pH 3.0	pH 7.0	pH 10.0	pH 3.0	pH 7.0	pH 10.0
(i) C_m (M)	2.2 ± 0.2	2.9 ± 0.3	2.9 ± 0.2	3.6 ± 0.5	3.9 ± 0.4	3.7 ± 0.4
(ii) $\Delta G°(H_2O)$ (kJ·mol^{-1})	16.3 ± 0.8	21.1 ± 1.2	16.6 ± 0.7	14.1 ± 0.9	15.4 ± 0.9	14.6 ± 0.6
(iii) m (kJ·mol^{-1}·M^{-1})	7.3 ± 0.4	7.2 ± 0.4	5.8 ± 0.2	3.9 ± 0.3	3.9 ± 0.2	3.9 ± 0.2
solvent-accessible surface ($Å^2$)	5844[b]			5187 ± 93[a]		
hydrophobic cavity volume ($Å^3$)	330 ± 44			510 ± 45		

[a] Result from analyses of 12 lowest energy structures of Mb nsLTP1. [b] Result was calculated from the X-ray determined structure (PDB ID: 1RZL).

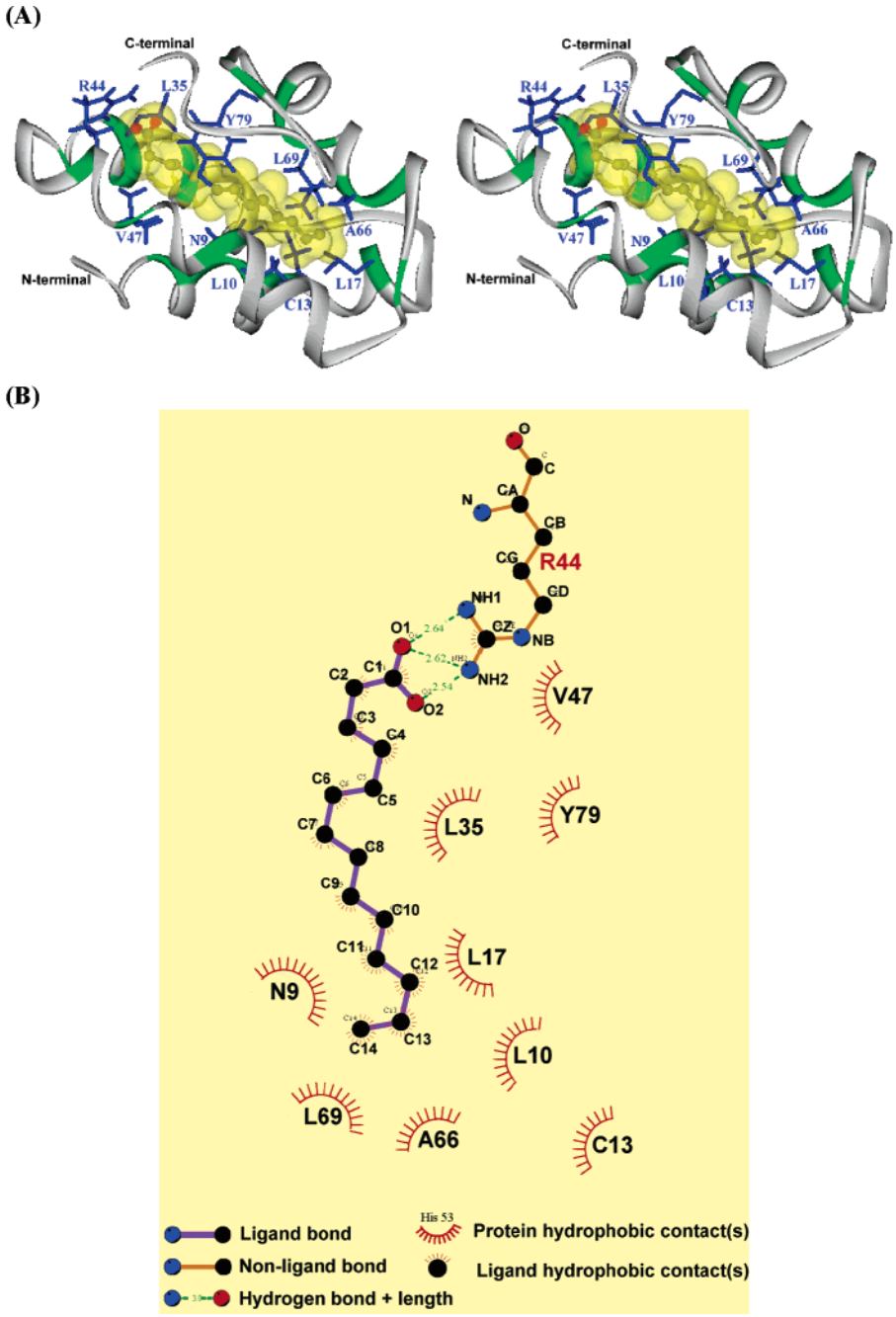

FIGURE 7: (A) Stereoview of the model of a Mb nsLTP1−myristate complex. Residues involved in the binding cavity are colored in green. The residues that interact with the ligand are shown in blue stick representation. The modeled ligand, myristate, is shown in ball-and-stick representation and the backbone of Mb nsLTP1 in ribbon representation. (B) Intermolecular interactions between Mb nsLTP1 and myristate. The figure was generated using Ligplot v.4.0 (*43*).

of rice and Mb nsLTP1 were studied with fluorescence spectroscopy by monitoring the increase in fluorescence due to the transfer of pyrene moieties from quenched donor vesicles to unquenched acceptor vesicles (*50*). The addition of protein (Mb or rice nsLTP1) to the sample induces a gradual increase in fluorescence intensity (Figure 6). In contrast to the previous comparison of lipid transfer properties of maize and wheat nsLTP1s whose activities are related to their respective cavity volume (*49*), Mb and rice nsLTP1s show similar lipid transfer activities, albeit a significant 35% smaller hydrophobic cavity of the latter (see previous section). To address whether disulfide bonds play an essential role in stabilizing the active conformation of Mb nsLTP1, lipid transfer activities of cysteine-modified Mb and rice nsLTP1 were measured. Lipid transfer activity was eliminated by reduction and modification of the disulfide bonds (data not shown). This indicates that the disulfide bond-stabilized structure is a prerequisite for lipid transfer activity.

To gain further insights into the lipid binding mode of Mb nsLTP1, we performed in silicon docking of a fatty acid into the hydrophobic cavity of Mb nsLTP1. This cavity is indeed a plausible ligand binding site. Docking of a myristate molecule into the hydrophobic cavity of Mb nsLTP1 results in an expansion of the cavity volume from 510 to 1142 Å^3. A similar result was observed in the rice nsLTP1−myristate complex (PDB ID: 1UVA) (*48*), whose hydrophobic cavity volume is 1100 Å^3. The lipid molecule is enclosed by the four helices of Mb nsLTP1 which form a hydrophobic cavity

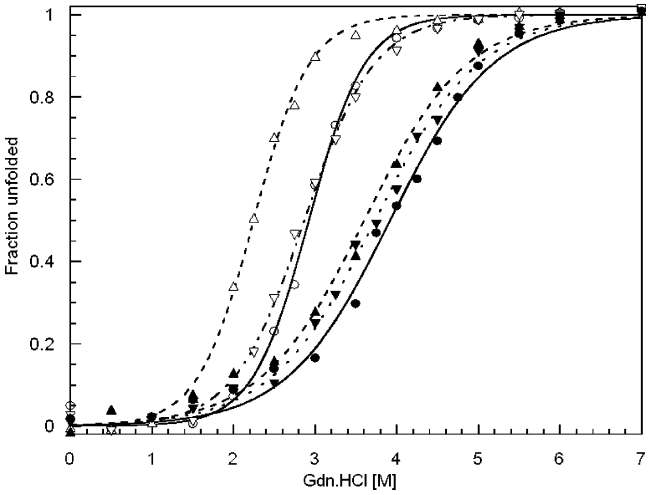

FIGURE 8: Chemical denaturations of Mb and rice nsLTP1s. Normalized CD signals at 222 nm are displayed as a function of increasing Gdn·HCl at pH 3.0 (regular triangle), pH 7.0 (circle), and pH 10.0 (inverted triangle) for Mb nsLTP1 (filled symbols) and rice nsLTP1 (open symbols). The curves were fitted with the nonlinear least-squares analysis according to a two-state model to show the fraction of unfolded.

with the following residues: Val[6], Asn[9], Leu[10], Cys[13], and Leu[17] of helix I; Val[31], Ile[34], and Leu[35] of helix II; Val[47] and Leu[51] of helix III; Ile[61], Asn[65], Ala[66], Leu[69], and Pro[70] of helix IV; and Ile[77] and Tyr[79] of the C-terminal region. The myristate is positioned similarly to those in complex with other nsLTP1s with a 1:1 binding mode (*24*, *48*). The polar head of the myristate lies in the cavity opening near the C-terminal part of Mb nsLTP1, whereas its hydrophobic tail points toward loop L3 (Figure 7). This model reveals some potential protein−ligand interaction sites similar to the ones observed in the rice nsLTP1−ligand complex. Leu[10], Cys[13], Leu[17], Ala[66], and Leu[69] interact with the aliphatic atoms C10 to C14 of the myristate at the bottom of the binding pocket while Asn[9], Leu[35], Val[47], and Tyr[79] are in close contact with the aliphatic atoms C2 to C9. Arg[44], on the other hand, forms the lid of the cavity and interacts with the headgroup of myristate. In conclusion, Mb and rice nsLTP1−myristate complexes display similar organization and volume of the internal hydrophobic cavity. Upon ligand binding, the hydrophobic cavities of both proteins expend. These results imply that the plasticity of nsLTP1s is essential for the formation of nsLTP1−lipid complexes and accounts for the similar lipid transfer activities.

Comparisons of the Thermodynamic Properties of Rice and Mb nsLTP1. The protein stability has been shown to decrease with the increasing size of the hydrophobic cavity (*51*, *52*). To study the relationship between hydrophobic cavity size and structural stability, the thermodynamic properties of Mb and rice nsLTP1s were compared using CD spectroscopy. Normalized CD spectra at three pH values between 3.0 and 10.0 are shown in Figure 8. Mb nsLTP1 requires a higher concentration of Gdn·HCl (6.5 M) than rice nsLTP1 (4.5 M) to be fully denatured. We used nonlinear least-squares regression to fit the chemical-induced unfolding data (*53*). Thermodynamic parameters were derived under the assumption of a two-state model (Table 3), and the results revealed that both Mb and rice nsLTP1s exhibit maximum stability around neutral pH. Note that Mb nsLTP1 is less stable than rice nsLTP1 [$\Delta\Delta G°(H_2O) = 5.7$ kJ·mol^{-1}; see Table 3] although it requires a higher denaturant concentration (C_m) to unfold. C_m is related to the m value according to the equation

$$\Delta G° = \Delta G°(H_2O) + m[\text{denaturant}] \qquad (3)$$

where m is a measure of the cooperativity of the unfolding process and is proportional to the surface area exposed to solvent upon unfolding (*54*). The absolute m value of Mb (3.9 kJ·mol^{-1}·M^{-1}) is smaller than that of rice nsLTP1 (7.2 kJ·mol^{-1}·M^{-1}) (Table 3). This is in agreement with the solvent-accessible surface areas of Mb and rice nsLTP1s, which are 5187 ± 93 and 5844 Å^2, respectively. Briefly, the lower m value suggests that the transition from the folded to the unfolded state of Mb nsLTP1 is less cooperative than that of rice (*55*). Mb nsLTP1 has a lower $\Delta G°(H_2O)$ than rice nsLTP1, which is consistent with hydrophobic cavity values calculated from their structures.

Probable Role of nsLTP1 as Plant Defensin. Next to their passive role of nsLTP1s in formation of structural barriers such as cutin, they are found to exhibit an active role in plant defense (*13*). They show antimicrobial activities, and some nsLTP1s genes are inducible upon pathogen attack (*13*). Accumulation of nsLTP1s at the plant surface site in contact with fungi (*56*−*58*) is evidence of their role in plant defense. In addition, nsLTP1s can work in synergy with thionin, a plant defense peptide, to inhibit fungi growth (*59*). Recently, Mb nsLTP1 has been shown to exert antifungal action toward *Fusarium solani*, *Fusarium oxysporum*, *Pythium aphanidermatum*, and *Sclerotium rolfsii* (*28*). Coincubation of Mb nsLTP1 with the Gram-positive bacteria such as *Staphylococcus aureus* can cause cytoplasmic leakage in vitro (*28*). Unlike wheat nsLTP1, which acts as an elicitin antagonist (*4*), Mb nsLTP1 kills bacteria by destructing their cell wall (*28*). Either the 3D structure or the antimicrobial activities of nsLTP homologues have been reported previously. We have shown here, for the first time, the solution structure of a nsLTP1 from Mb with known antimicrobial activity (*28*). The antimicrobial activity may be attributed to the amphipathic nature of Mb nsLTP1, on the surface of which a basic patch is formed by clustered cationic residues (Figure 5D). Clustered distributions of cationic and hydrophobic residues are common features of antimicrobial peptides (*60*). Like several known plant defensive peptides, the positively charged face may bind to the negatively charged membrane surface of microorganisms (*61*). Our structure may thus shed new light on the structure−function relationship of nsLTPs' antimicrobial activity.

CONCLUSIONS

We have described the purification, identification, and 3D structure determination of nsLTP1 from Mb sprout with structural characteristics of the lipid transfer protein family. Its thermostability (T_m > 80 °C), lipid transfer activity, and 3D structure highly resemble the maize and rice nsLTP1s, implying that nsLTP1s of monocotyledonous and dicotyledonous plants may play a similar role in managing stresses and defending pathogens. Although the volume and organization of the internal cavity exhibit subtle differences from one nsLTP1 to another, similar lipid transfer activities suggest that their plasticity rather than the volume of their hydrophobic cavity is a determinant of their ability to transfer lipids.

The hydrophobic interior of proteins is usually believed to be tightly packed and has been shown to have very low compressibility (*62*). The presence of a large internal cavity in nsLTP1s is quite remarkable in terms of folding and stability. Our denaturant-induced unfolding assay has revealed that Mb nsLTP1 is less stable and shows less cooperative unfolding than rice nsLTP1. Despite the similar global 3D structures among several nsLTP1s, minor/local structural differences influence their stability and folding. The structural features of Mb nsLTP1 should provide new insights into their biological role in the defense against plant pathogens. A more systematic analysis of the structures and corresponding lipid binding/transfer properties as well as antimicrobial activity should clarify the biological role(s) of this class of proteins.

ACKNOWLEDGMENT

The authors acknowledge the support of the Regional Instrument Center, Department of Life Sciences, for the sequencing and amino acid composition experiments.

SUPPORTING INFORMATION AVAILABLE

Diagrams showing the number of constraints per residue, local RMSD, the sequential assignment of the $H^{\alpha}(i)-H^{N}(i+1)$ cross-peaks in the fingerprint region, and a summary of the sequential assignment and secondary structure constraints of Mb nsLTP1. This material is available free of charge via the Internet at http://pubs.acs.org.

REFERENCES

1. Kader, J. C. (1996) Lipid transfer proteins in plants, *Annu. Rev. Plant Physiol. Plant Mol. Biol. 47*, 627−654.
2. Sterk, P., Booij, H., Schellekens, G. A., Van Kammen, A., and De Vries, S. C. (1991) Cell-specific expression of the carrot EP2 lipid transfer protein gene, *Plant Cell 3*, 907−921.
3. Garcia-Olmedo, F., Molina, A., Segura, A., and Moreno, M. (1995) The defensive role of nonspecific lipid-transfer proteins in plants, *Trends Microbiol. 3*, 72−74.
4. Buhot, N., Douliez, J. P., Jacquemard, A., Marion, D., Tran, V., Maume, B. F., Milat, M. L., Ponchet, M., Mikes, V., Kader, J. C., and Blein, J. P. (2001) A lipid transfer protein binds to a receptor involved in the control of plant defence responses, *FEBS Lett. 509*, 27−30.
5. Park, S. Y., and Lord, E. M. (2003) Expression studies of SCA in lily and confirmation of its role in pollen tube adhesion, *Plant Mol. Biol. 51*, 183−189.
6. Edqvist, J., and Farbos, I. (2002) Characterization of germination-specific lipid transfer proteins from *Euphorbia lagascae*, *Planta 215*, 41−50.
7. Trevino, M. B., and O'Connell, M. A. (1998) Three drought-responsive members of the nonspecific lipid-transfer protein gene family in *Lycopersicon pennellii* show different developmental patterns of expression, *Plant Physiol. 116*, 1461−1468.
8. Torres-Schumann, S., Godoy, J. A., and Pintor-Toro, J. A. (1992) A probable lipid transfer protein gene is induced by NaCl in stems of tomato plants, *Plant Mol. Biol. 18*, 749−757.
9. Dunn, M. A., Hughes, M. A., Zhang, L., Pearce, R. S., Quigley, A. S., and Jack, P. L. (1991) Nucleotide sequence and molecular analysis of the low-temperature induced cereal gene, BLT4, *Mol. Gen. Genet. 229*, 389−394.
10. Hoffmann-Sommergruber, K. (2000) Plant allergens and pathogenesis-related proteins. What do they have in common?, *Int. Arch. Allergy Immunol. 122*, 155−166.
11. Douliez, J. P., Michon, T., Elmorjani, K., and Marion, D. (2000) Structure, biological and technological functions of lipid transfer proteins and indolines, the major lipid binding proteins from cereal kernels, *J. Cereal Sci. 32*, 1−20.
12. Kalla, R., Shimamoto, K., Potter, R., Nielsen, P. S., Linnestad, C., and Olsen, O. A. (1994) The promoter of the barley aleurone-specific gene encoding a putative 7 kDa lipid transfer protein confers aleurone cell-specific expression in transgenic rice, *Plant J. 6*, 849−860.
13. Guiderdoni, E., Cordero, M. J., Vignols, F., Garcia-Garrido, J. M., Lescot, M., Tharreau, D., Meynard, D., Ferriere, N., Notteghem, J. L., and Delseny, M. (2002) Inducibility by pathogen attack and developmental regulation of the rice Ltp1 gene, *Plant Mol. Biol. 49*, 683−699.
14. Gincel, E., Simorre, J. P., Caille, A., Marion, D., Ptak, M., and Vovelle, F. (1994) Three-dimensional structure in solution of a wheat lipid-transfer protein from multidimensional ^{1}H NMR data. A new folding for lipid carriers, *Eur. J. Biochem. 226*, 413−422.
15. Shin, D. H., Lee, J. Y., Hwang, K. Y., Kim, K. K., and Suh, S. W. (1995) High-resolution crystal structure of the non-specific lipid-transfer protein from maize seedlings, *Structure 3*, 189−199.
16. Heinemann, B., Andersen, K. V., Nielsen, P. R., Bech, L. M., and Poulsen, F. M. (1996) Structure in solution of a four-helix lipid binding protein, *Protein Sci. 5*, 13−23.
17. Gomar, J., Petit, M. C., Sodano, P., Sy, D., Marion, D., Kader, J. C., Vovelle, F., and Ptak, M. (1996) Solution structure and lipid binding of a nonspecific lipid transfer protein extracted from maize seeds, *Protein Sci. 5*, 565−577.
18. Lerche, M. H., Kragelund, B. B., Bech, L. M., and Poulsen, F. M. (1997) Barley lipid-transfer protein complexed with palmitoyl CoA: the structure reveals a hydrophobic binding site that can expand to fit both large and small lipid-like ligands, *Structure 5*, 291−306.
19. Lee, J. Y., Min, K., Cha, H., Shin, D. H., Hwang, K. Y., and Suh, S. W. (1998) Rice non-specific lipid transfer protein: the 1.6 Å crystal structure in the unliganded state reveals a small hydrophobic cavity, *J. Mol. Biol. 276*, 437−448.
20. Lerche, M. H., and Poulsen, F. M. (1998) Solution structure of barley lipid transfer protein complexed with palmitate. Two different binding modes of palmitate in the homologous maize and barley nonspecific lipid transfer proteins, *Protein Sci. 7*, 2490−2498.
21. Poznanski, J., Sodano, P., Suh, S. W., Lee, J. Y., Ptak, M., and Vovelle, F. (1999) Solution structure of a lipid transfer protein extracted from rice seeds. Comparison with homologous proteins, *Eur. J. Biochem. 259*, 692−708.
22. Charvolin, D., Douliez, J. P., Marion, D., Cohen-Addad, C., and Pebay-Peyroula, E. (1999) The crystal structure of a wheat nonspecific lipid transfer protein (ns-LTP1) complexed with two molecules of phospholipid at 2.1 Å resolution, *Eur. J. Biochem. 264*, 562−568.
23. Tassin-Moindrot, S., Caille, A., Douliez, J. P., Marion, D., and Vovelle, F. (2000) The wide binding properties of a wheat nonspecific lipid transfer protein. Solution structure of a complex with prostaglandin B2, *Eur. J. Biochem. 267*, 1117−1124.
24. Han, G. W., Lee, J. Y., Song, H. K., Chang, C., Min, K., Moon, J., Shin, D. H., Kopka, M. L., Sawaya, M. R., Yuan, H. S., Kim, T. D., Choe, J., Lim, D., Moon, H. J., and Suh, S. W. (2001) Structural basis of non-specific lipid binding in maize lipid-transfer protein complexes revealed by high-resolution X-ray crystallography, *J. Mol. Biol. 308*, 263−278.
25. Pastorello, E. A., Farioli, L., Pravettoni, V., Giuffrida, M. G., Ortolani, C., Fortunato, D., Trambaioli, C., Scibola, E., Calamari, A. M., Robino, A. M., and Conti, A. (2001) Characterization of the major allergen of plum as a lipid transfer protein, *J. Chromatogr., B: Biomed. Sci. Appl. 756*, 95−103.
26. Conti, A., Fortunato, D., Ortolani, C., Giuffrida, M. G., Pravettoni, V., Napolitano, L., Farioli, L., Perono Garoffo, L., Trambaioli, C., and Pastorello, E. A. (2001) Determination of the primary structure of two lipid transfer proteins from apricot (*Prunus armeniaca*), *J. Chromatogr., B: Biomed. Sci. Appl. 756*, 123−129.
27. Pastorello, E. A., Ortolani, C., Baroglio, C., Pravettoni, V., Ispano, M., Giuffrida, M. G., Fortunato, D., Farioli, L., Monza, M., Napolitano, L., Sacco, M., Scibola, E., and Conti, A. (1999) Complete amino acid sequence determination of the major allergen of peach (*Prunus persica*) Pru p 1, *Biol. Chem. 380*, 1315−1320.
28. Wang, S. Y., Wu, J. H., Ng, T. B., Ye, X. Y., and Rao, P. F. (2004) A non-specific lipid transfer protein with antifungal and antibacterial activities from the mung bean, *Peptides 25*, 1235−1242.
29. Liu, Y. J., Samuel, D., Lin, C. H., and Lyu, P. C. (2002) Purification and characterization of a novel 7-kDa non-specific

lipid transfer protein-2 from rice (*Oryza sativa*), *Biochem. Biophys. Res. Commun. 294*, 535−540.
30. Coligan, J. E., Dunn, B. M., Ploegh, H. L., Speicher, D. W., and Wingfield, P. T. (1998) *Currently Protocols in Protein Science*, J. Wiley & Sons, New York.
31. Edman, P., and Begg, G. (1967) A protein sequenator, *Eur. J. Biochem. 1*, 80−91.
32. Smith, P. K., Krohn, R. I., Hermanson, G. T., Mallia, A. K., Gartner, F. H., Provenzano, M. D., Fujimoto, E. K., Goeke, N. M., Olson, B. J., and Klenk, D. C. (1985) Measurement of protein using bicinchoninic acid, *Anal. Biochem. 150*, 76−85.
33. Gans, P. J., Lyu, P. C., Manning, M. C., Woody, R. W., and Kallenbach, N. R. (1991) The helix-coil transition in heterogeneous peptides with specific side-chain interactions: theory and comparison with CD spectral data, *Biopolymers 31*, 1605−1614.
34. Kamal, J. K., and Behere, D. V. (2002) Thermal and conformational stability of seed coat soybean peroxidase, *Biochemistry 41*, 9034−9042.
35. Goddard, T. D., and Kneller, D. G. (1999) SPARKY3, University of California, San Francisco.
36. Brunger, A. T., Adams, P. D., Clore, G. M., Delano, W. L., Gros, P., Grosse-Kunstleve, R. W., Jiang, J. S., Kuszewski, J., Nilges, M., Pannu, N. S., Read, R. J., Rice, L. M., Simonson, T., and Warren, G. L. (1998) Crystallography & NMR System, *Acta Crystallogr. D54*, 905−921.
37. Nilges, M., Macias, M. J., O'Donoghue, S. I., and Oschkinat, H. (1997) Automated NOESY interpretation with ambiguous distance restraints: the refined NMR solution structure of the pleckstrin homology domain from beta-spectrin, *J. Mol. Biol. 269*, 408−422.
38. Linge, J. P., Williams, M. A., Spronk, C. A., Bonvin, A. M., and Nilges, M. (2003) Refinement of protein structures in explicit solvent, *Proteins 50*, 496−506.
39. Laskowski, R. A., MacArthur, M. W., Moss, D. S., and Thornton, J. M. (1993) PROCHECK: a program to check the stereochemical quality of protein, *J. Appl. Crystallogr.*, 283−291.
40. Guex, N., and Peitsch, M. C. (1997) SWISS-MODEL and the Swiss-PdbViewer: an environment for comparative protein modeling, *Electrophoresis 18*, 2714−2723.
41. Kleywegt, G. J., and Jones, T. A. (1994) Detection, delineation, measurement and display of cavities in macromolecular structures, *Acta Crystallogr. D50*, 178−185.
42. Sanner, M. F., Olson, A. J., and Spehner, J. C. (1996) Reduced surface: an efficient way to compute molecular surfaces, *Biopolymers 38*, 305−320.
43. Wallace, A. C., Laskowski, R. A., and Thornton, J. M. (1995) LIGPLOT: a program to generate schematic diagrams of protein−ligand interactions, *Protein Eng. 8*, 127−134.
44. Samuel, D., Liu, Y. J., Cheng, C. S., and Lyu, P. C. (2002) Solution structure of plant nonspecific lipid transfer protein-2 from rice (*Oryza sativa*), *J. Biol. Chem. 277*, 35267−35273.
45. Wuthrich, K. (1986) *NMR of Proteins and Nucleic Acids*, J. Wiley & Sons, New York.
46. Tassin, S., Broekaert, W. F., Marion, D., Acland, D. P., Ptak, M., Vovelle, F., and Sodano, P. (1998) Solution structure of Ace-AMP1, a potent antimicrobial protein extracted from onion seeds. Structural analogies with plant nonspecific lipid transfer proteins, *Biochemistry 37*, 3623−3637.
47. Baud, F., Pebay-Peyroula, E., Cohen-Addad, C., Odani, S., and Lehmann, M. S. (1993) Crystal structure of hydrophobic protein from soybean; a member of a new cysteine-rich family, *J. Mol. Biol. 231*, 877−887.
48. Cheng, H. C., Cheng, P. T., Peng, P., Lyu, P. C., and Sun, Y. J. (2004) Lipid binding in rice nonspecific lipid transfer protein-1 complexes from *Oryza sativa*, *Protein Sci. 13*, 2304−2315.
49. Guerbette, F., Grosbois, M., Jolliot-Croquin, A., Kader, J. C., and Zachowski, A. (1999) Comparison of lipid binding and transfer properties of two lipid transfer proteins from plants, *Biochemistry 38*, 14131−14137.
50. van Paridon, P. A., Gadella, T. W., Jr., Somerharju, P. J., and Wirtz, K. W. (1988) Properties of the binding sites for the sn-1 and sn-2 acyl chains on the phosphatidylinositol transfer protein from bovine brain, *Biochemistry 27*, 6208−6214.
51. Eriksson, A. E., Baase, W. A., Zhang, X. J., Heinz, D. W., Blaber, M., Baldwin, E. P., and Matthews, B. W. (1992) Response of a protein structure to cavity-creating mutations and its relation to the hydrophobic effect, *Science 255*, 178−183.
52. Xu, J., Baase, W. A., Baldwin, E., and Matthews, B. W. (1998) The response of T4 lysozyme to large-to-small substitutions within the core and its relation to the hydrophobic effect, *Protein Sci. 7*, 158−177.
53. Santoro, M. M., and Bolen, D. W. (1988) Unfolding free energy changes determined by the linear extrapolation method. 1. Unfolding of phenylmethanesulfonyl alpha-chymotrypsin using different denaturants, *Biochemistry 27*, 8063−8068.
54. Agashe, V. R., and Udgaonkar, J. B. (1995) Thermodynamics of denaturation of barstar: evidence for cold denaturation and evaluation of the interaction with guanidine hydrochloride, *Biochemistry 34*, 3286−3299.
55. Sivaraman, T., Kumar, T. K., Tu, Y. T., Peng, H. J., and Yu, C. (1999) Structurally homologous toxins isolated from the Taiwan cobra (*Naja naja atra*) differ significantly in their structural stability, *Arch. Biochem. Biophys. 363*, 107−115.
56. Molina, A., and Garcia-Olmedo, F. (1993) Developmental and pathogen-induced expression of three barley genes encoding lipid transfer proteins, *Plant J. 4*, 983−991.
57. Carvalho, A. O., Machado, O. L. T., Cunha, M. D., Santos, I. S., and Gomes, V. M. (2001) Antimicrobial peptides and immunolocalization of a LTP in *Vigna unguiculata* seeds, *Plant Physiol. Biochem. 39*, 137−146.
58. Nielsen, K. K., Nielsen, J. E., Madrid, S. M., and Mikkelsen, J. D. (1996) New antifungal proteins from sugar beet (*Beta vulgaris* L.) showing homology to non-specific lipid transfer proteins, *Plant Mol. Biol. 31*, 539−552.
59. Segura, A., Moreno, M., and Garcia-Olmedo, F. (1993) Purification and antipathogenic activity of lipid transfer proteins (LTPs) from the leaves of Arabidopsis and spinach, *FEBS Lett. 332*, 243−246.
60. Zasloff, M. (2002) Antimicrobial peptides of multicellular organisms, *Nature 415*, 389−395.
61. De Samblanx, G. W., Goderis, I. J., Thevissen, K., Raemaekers, R., Fant, F., Borremans, F., Acland, D. P., Osborn, R. W., Patel, S., and Broekaert, W. F. (1997) Mutational analysis of a plant defensin from radish (*Raphanus sativus* L.) reveals two adjacent sites important for antifungal activity, *J. Biol. Chem. 272*, 1171−1179.
62. Morozov, V. N., and Morozova, T. (1986) Thermal motion of whole protein molecule in proteins solids, *J. Theor. Biol. 121*, 73−88.
63. Jorgensen, W. L., and Tirado-Rives, J. (1988) The OPLS potential functions for proteins. Energy minimizations for crystals of cyclin peptides and crambin, *J. Am. Chem. Soc. 110*, 1657−1666.

BI047608V